Modeling Tropical Cyclone Boundary Layer: Height-Resolving Pressure and Wind Fields

Reda Snaiki, Teng Wu*

Department of Civil, Structural and Environmental Engineering, University at Buffalo, State University of New York, Buffalo, NY 14126, USA

**Corresponding author. Email:* tengwu@buffalo.edu

Abstract: The high-accurate wind field of a tropical cyclone boundary layer, which is essentially governed by the Navier-Stokes equations, could be efficiently obtained by predefining the pressure field. Conventionally, the prescribed pressure filed is a 1-D function varying with the distance to the cyclone center (radius). In this study, the pressure field model has been extended to a 2-D function with respect to both radius and height. In addition, a number of field measurements in the tropical cyclone boundary layer indicate rapid variation of the thermodynamic temperature and moisture with time and space. Hence, their effects on the wind field were considered in terms of the virtual temperature, which was integrated in the modeling of pressure field. The analytical solutions of the wind field, as a sum of gradient and frictional wind components, were derived based on a height-resolving scheme using the updated pressure field. Since the tropical cyclone gradient wind and depth of boundary layer are mutually dependent, the iteration approach was utilized in the computation. The proposed height-resolving pressure and wind analytical models have been comprehensively validated with the global positioning system (GPS)-based dropsonde data. The significant importance to consider the height-varying pressure, thermodynamic temperature and moisture in the modeling of the wind field in the tropical cyclone boundary layer were also demonstrated.

Keywords: *Tropical cyclone, Height-resolving model, Boundary layer wind, Pressure, Temperature, Moisture.*

1. Introduction

The wind field in the boundary layer region of a mature tropical cyclone is of great significance since a substantial part of economic and life losses result from the events directly or indirectly related to high winds, e.g., wind damage to structures, wind-driven storm surge and wind-rainfall interaction. The situation has become more challenging due to the changing climate and continued escalation of coastal population. While there have been considerable advances in improving the simulation accuracy of tropical cyclone wind field based on the numerical weather prediction models associated with a significant increase of observation data, they are not practical to be employed in the assessments of risk posted by wind-related hazards due to their high computational demands. The state-of-the-art wind hazard risk analysis is essentially based on the Monte Carlo methodology proposed by Russel (1971), where a large number of scenarios need to be carried out. In this context, the parametric, engineering models for tropical cyclone wind fields, based on the prescribed pressure fields, have been popularly utilized.

While several studies have shown that the height-resolving models are superior to the slab (depth-averaged) models that treat the boundary-layer height of the tropical cyclone as a constant, both of these two high-efficient wind field simulation schemes are widely employed in engineering applications. Although the hydrostatic equation simply indicates the pressure field depends on the height, both the slab and height-resolving models conventionally assume the prescribed pressure field is unchanged through the depth of the boundary layer. In particular, the 1-D empirical model introduced by Holland (1980) for pressure, varying with the distance to the cyclone center (radius), has been extensively used due to its simplicity and consistency with field measurements (e.g., Zhao et al. 2013; Mudd et al. 2014). Recently, Huang et al. (2012) integrated the effects of temperature and variation of central pressure difference with height into the prescribed pressure field for more

accurately simulating the typhoon wind field using Meng's model (Meng et al. 1995). Since the gradient wind speed in this refined Meng's model varies with the height from the ground, it is not easy to select the appropriate value in the calculation.

Following the pioneering work of Huang et al. (2012), the 1-D Holland's empirical pressure model has been extended to a 2-D function with respect to both radius and height in this study. Since a number of field measurements in the tropical cyclone boundary layer indicate rapid variation of the thermodynamic temperature and moisture with time and space, their effects on the wind field were considered in terms of the virtual temperature, which was integrated in the modeling of pressure field. The obtained 2-D formula for pressure $p(z,r)$ explicitly includes the temperature lapse rate parameter Γ. The global positioning system (GPS)-based dropsonde data (e.g., temperature, humidity, pressure) for the tropical cyclones further demonstrated a heavy dependence of Γ and hence pressure on the moisture content. Furthermore, the proposed 2-D pressure formula indicates the consideration of climate changes (e.g., global warming) may have significant implications to the wind field simulation of a tropical cyclone. The analytical solutions of the wind field were derived based on a recently developed height-resolving scheme (Snaiki and Wu 2016) using the obtained 2-D pressure field. To select an appropriate height for the calculation of gradient wind speed, the iteration approach was utilized using the depth scale of the tropical cyclone boundary layer as the initial value. The proposed height-resolving pressure and wind analytical models have been comprehensively validated with the GPS-based dropsonde data. The significant importance to consider the height-varying pressure, thermodynamic temperature and moisture in the modeling of the wind field in the tropical cyclone boundary layer were also demonstrated.

2. Height-resolving pressure field

In the simulation of the wind field inside the boundary layer of a tropical cyclone, the surface level pressure profile is typically prescribed to efficiently solve the horizontal momentum equations. In general, the atmospheric pressure can be expressed by the state equation for ideal gas as follows:

$$p = \rho R T \tag{1}$$

where ρ = air density; R = ideal gas constant; and T = temperature.

2.1 Moisture effects

The warm, moist air is considered as the fuel of the tropical cyclones. To simultaneously account for the temperature and moisture effects, a convenient way to proceed would be the use of the virtual temperature T_v which is expressed as follows:

$$T_v = T\left[\frac{R_{noa} + r_v R_v}{R_{noa}\left(1 + r_v\right)}\right] \tag{2}$$

where r_v = mixing ratio of water vapor; R_v = gas constant of the water vapor; and $R_{noa} \approx 287\, J\, kg^{-1} K^{-1}$ is the gas constant of mixture of nitrogen (N_2), oxygen (O_2) and argon (Ar). R_{noa} will be denoted subsequently by R for convenience. Accordingly, the state equation can be extended to include the virtual temperature:

$$p = \rho R T_v \tag{3}$$

The importance of moisture consideration in the pressure simulation for a typical tropical cyclone will be illustrated through two dropsonde measurements collected by the National Hurricane Center and Hurricane Research Division during hurricane Katrina. The dropsonde IDs are (051926111) and (051926170), respectively. The dropsondes are usually launched from an

altitude of 3 km or higher and provide high-resolution thermodynamics data, namely temperature, pressure, and humidity. To ensure quality control, collected data are post-processed. Figure 1 presents the pressure p as a function of $\rho_{humid\ air} * T_v$ and of $\rho_{dry\ air} * T$, respectively. It is shown the consideration of moisture gives a slope of 285.6 that is close to the gas constant $R \approx 287\ J\ kg^{-1}K^{-1}$, while the dry assumption results in a slope much larger than this value. This indicates the importance of moisture to accurately simulate the pressure field in the tropical cyclone.

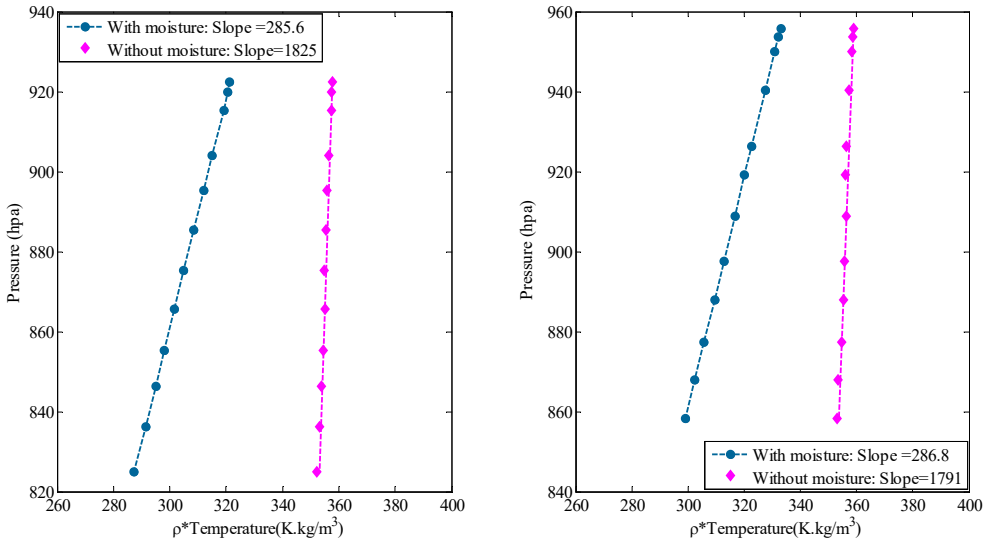

Fig. 1 Moisture effects on the state equation based on two dropsonde measurements during hurricane Katrina (Left: 051926170 and Right: 051926111)

2.2 Pressure formula

To derive the pressure expression, the state equation is first applied on the surface level which gives:

$$p_0 = \rho_0 R T_{v0} \tag{4}$$

where ρ_0 = surface air density; and T_{v0} =surface virtual temperature.

Combining the Eqs. (3) and (4) yields the following expression:

$$\frac{p}{p_0} = \frac{\rho T_v}{\rho_0 T_{v0}} \tag{5}$$

The surface pressure is given based on the widely-used Holland's formula:

$$p_0 = p_{c0} + \Delta p_0 . exp\left[-\left(r_m / r \right)^B \right] \tag{6}$$

where p_{c0} = central pressure at the surface; Δp_0 = central pressure difference at the surface; r_m = radius of maximum winds; r = radial distance from the tropical cyclone center; and B = Holland's radial pressure parameter. Hence the pressure can be expressed as:

$$p = \frac{\rho T_v}{\rho_0 T_{v0}} \left(p_{c0} + \Delta p_0 . exp\left[-\left(r_m / r \right)^B \right] \right) \tag{7}$$

On the other hand, it is well known that temperature of air decreases with height. More specifically, it is approximately a linear function of height for relatively low altitudes, as shown in Fig. 2. The data in Fig. 2 is provided by the dropsonde (01074007) during hurricane Katrina.

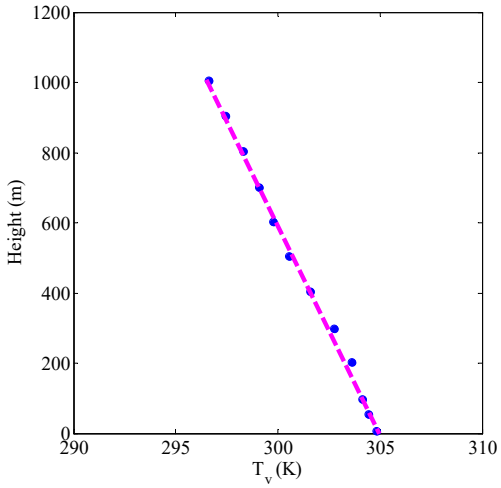

Fig. 2. Temperature profile of hurricane Katrina corresponding to the dropsonde ID (01074007)

Accordingly, the temperature could be approximated as:

$$T_v = -\Gamma z + T_{v0} \tag{8}$$

where z = vertical coordinate; and Γ = temperature lapse rate. Therefore, the pressure formula

becomes:

$$p = \frac{\rho}{\rho_0}\left(-\frac{\Gamma}{T_{v0}}z + 1\right)\left(p_{c0} + \Delta p_0 . exp\left[-\left(r_m / r\right)^B\right]\right) \tag{9}$$

If the moisture was disregarded, one could determine the value of the so-called dry adiabatic lapse rate for dry simulation according to the first law of thermodynamics $dq = c_p dT - \frac{1}{\rho}dp$, where c_p = specific heat capacity of air; dq = heat transfer =0; and $dp = -\rho g dz$ based on the hydrostatic equation. As a result, the dry adiabatic lapse rate can be obtained as follows:

$$\Gamma_d = -\frac{dT}{dz} = \frac{g}{c_p} \approx 9.8\, K/Km \tag{10}$$

For a typical tropical cyclone, however, it is noted that the temperature lapse rate changes with space. Hence, constant Γ_d cannot be adopted for the pressure simulation. Figure 3 presents the radial variation of the lapse rate for hurricane Gustav (2008) based on 62 dropsondes data.

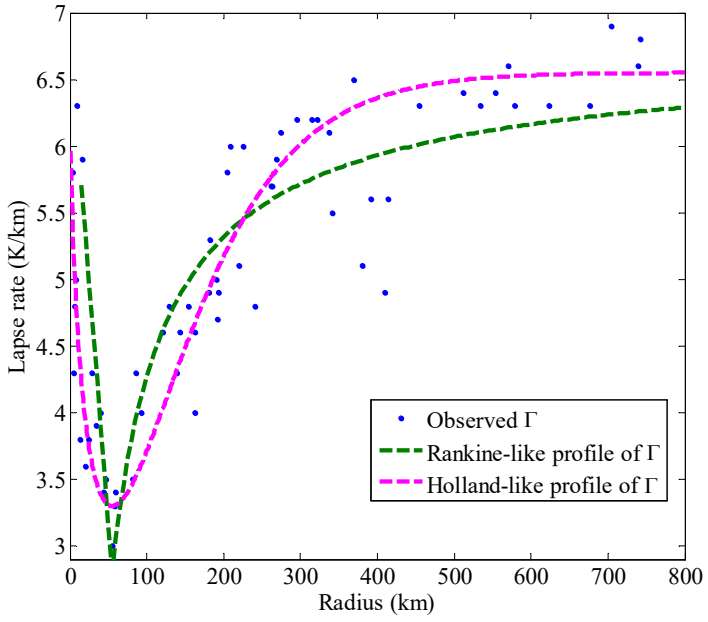

Fig. 3. Radial variation of the observed lapse rate for hurricane Gustav (2008)

As shown in Fig. 3, the lapse rate varies considerably with the distance from the center of the tropical cyclone. The variation is reasonable since the moisture causes the lapse rate to be smaller (CCSP 2006; IPCC 2000; 2007; 2012). Actually, the lapse rate parameter Γ is an important parameter in the meteorology science to consider the negative feedback from global warming and hence increased moisture (IPCC 2000; 2007; 2012). In the eyewall region where the moisture content is high, there is a rapid drop in the lapse rate (around $3\,K/km$). Then the moisture content tends to decrease far away from the eye wall, which leads to an increase of the lapse rate reaching a value around $6.5\,K/km$. Similarly, a reduced moisture content results in increase of the lapse rate in the eye region compared to the eye wall region. There is a sudden decrease of the lapse rate in some regions far away from the tropical cyclone center, as presented in Fig. 3 (around $r \approx 400\,km$). This is probably because these specific dropsondes were launched in a rainband region where the moisture content was locally increased. It should be noted that only the radial variation of the lapse rate is illustrated in Fig. 3, while, in general, it is also dependent on the azimuthal coordinate. The temperature lapse rate in the tropical cyclone is typically smaller than the dry adiabatic lapse rate $\Gamma_d \approx 9.8°K/Km$.

Based on the measured data shown in Fig. 3, two empirical radial profiles of Γ are proposed in this study for convenient applications to the pressure simulations in the tropical cyclone. The first formula is a modified version of Rankine-like profile, which leads to the following expression for the lapse rate:

$$\Gamma(r) = \begin{cases} (\Gamma_{r_m} - \Gamma_{eye})\dfrac{r}{r_m} + \Gamma_{eye} & ;\ r < r_m \\ (\Gamma_{r_m} - \Gamma_0)\left(\dfrac{r_m}{r}\right)^a + \Gamma_0 & ;\ r \geq r_m \end{cases} \tag{11}$$

where Γ_{r_m} = lapse rate at the radius of maximum winds; Γ_{eye} = lapse rate at the tropical cyclone center; Γ_0 = lapse rate in the far field; a = scaling parameter that adjusts the profile shape. The second formula can be obtained using a modified version of Holland-like profile, which leads to the following expression:

$$\Gamma(r) = \left(\Gamma_{rm} - \Gamma_0\right)\left\{\left(\frac{r_m}{r}\right)^b \exp\left[1-\left(\frac{r_m}{r}\right)^b\right]\right\}^{0.5} + \Gamma_0 \tag{12}$$

where b = scaling parameter that adjusts the profile shape; Γ_{eye} is assumed to be approximately equal to Γ_0 for simplification. In general, Eq. (12) provides a smoother profile than that generated by Eq. (11). The measured data of hurricane Gustav (2008) were fitted using the abovementioned empirical profiles [i.e., Eq. (11) and Eq. (12)] with parameters of $\Gamma_{r_m} = 2.8K/km$, $\Gamma_0 \approx \Gamma_{eye} \approx 6.8K/km$ and $a = 0.77$ for the Rankine-like profile and $\Gamma_{r_m} = 3.3K/km$, $\Gamma_0 = 6.55K/km$ and $b = 1.11$ for the Holland-like profile. The fitted profiles are shown in Fig. 3, and the one based on the Holland-like formula presents a better result according to least squares. It should be stressed out that the proposed empirical profiles of the lapse rate can be further improved with more data from the dropsondes.

Figures 4 and 5 present, respectively, the radial and vertical pressure profiles based on the proposed 2-D model [Eq. (9)] with various considerations of the lapse rates. The radial variation of the temperature lapse rates is obtained using the Holland-like profile. The other parameters are as follows: $p_{c0} = 950\,hpa$; $r_m = 55\,km$; $B = 1$; and $T_{v0} = 302\,K$. It is shown that the effects of the changing temperature lapse rate cannot be ignored to accurately simulate the pressure profiles in the tropical cyclones.

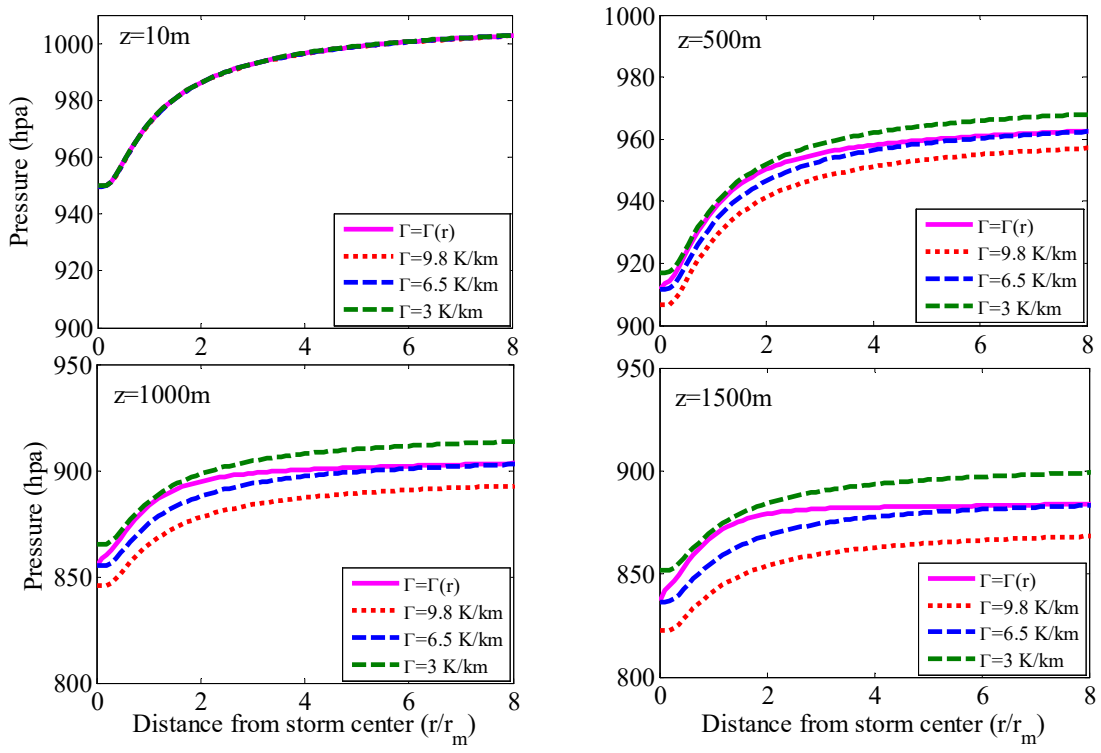

174

175 **Fig. 4.** Radial pressure profiles for several lapse rates at different altitudes

176 As shown in Fig. 4, the correlation of the radial pressure profile with the lapse rate increases with
177 the height. In the eyewall region, the proposed pressure profile $\left[\Gamma = \Gamma(r)\right]$ is almost identical to
178 the pressure profile corresponding to $\Gamma = 3\,K/km$, while it coincides with the pressure profile
179 corresponding to $\Gamma = 6.5K/km$ far away from the tropical cyclone center. This observation is
180 further demonstrated by the vertical pressure profiles as presented in Fig. 5. In addition, Fig. 5 also
181 clearly shows that larger differences of the pressure values are obtained at higher altitudes.

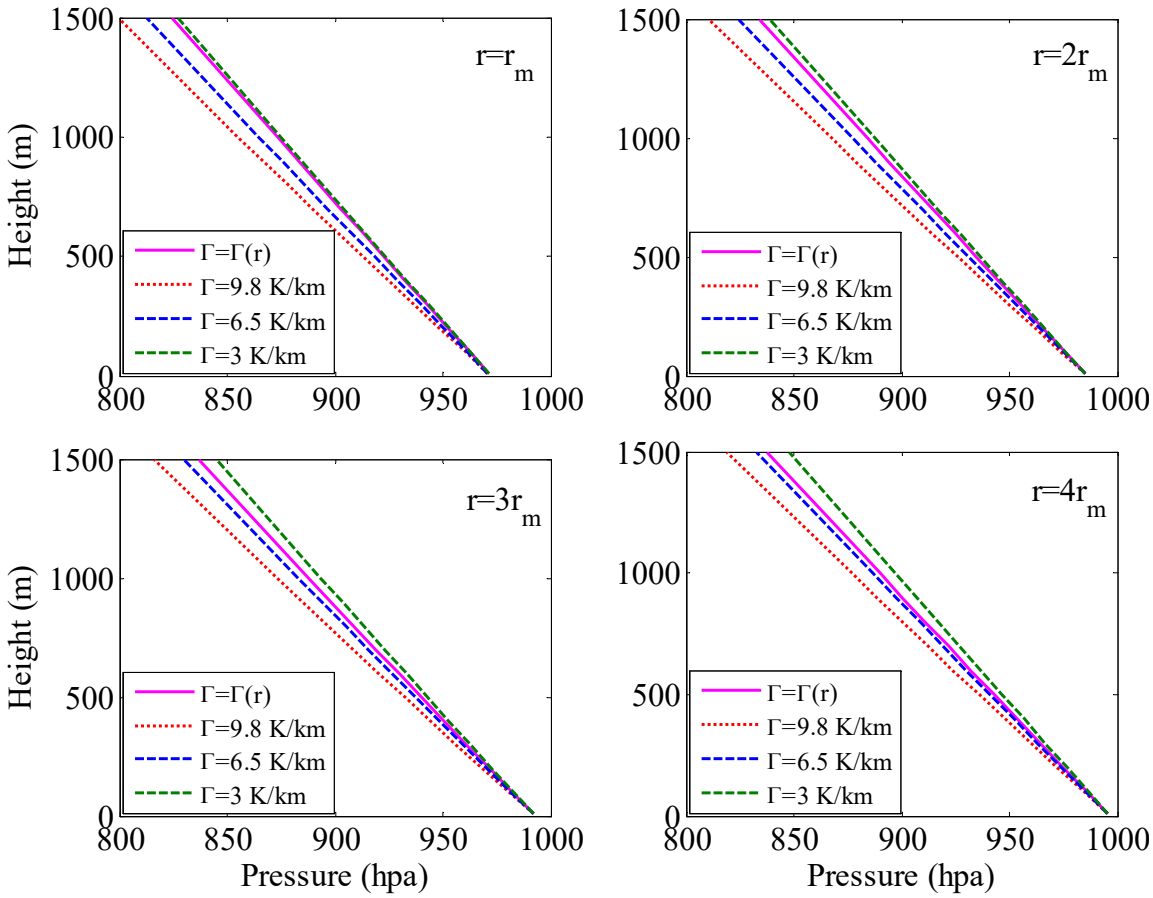

Fig. 5. Vertical Pressure profiles corresponding to several lapse rates at different locations inside the tropical cyclone

Using the same data as in Fig. 1, the vertical pressure profile was simulated using the proposed pressure profile [Eq. (9)]. It could be concluded that both the observed and simulated pressures are in good agreement as illustrated in Fig. 6.

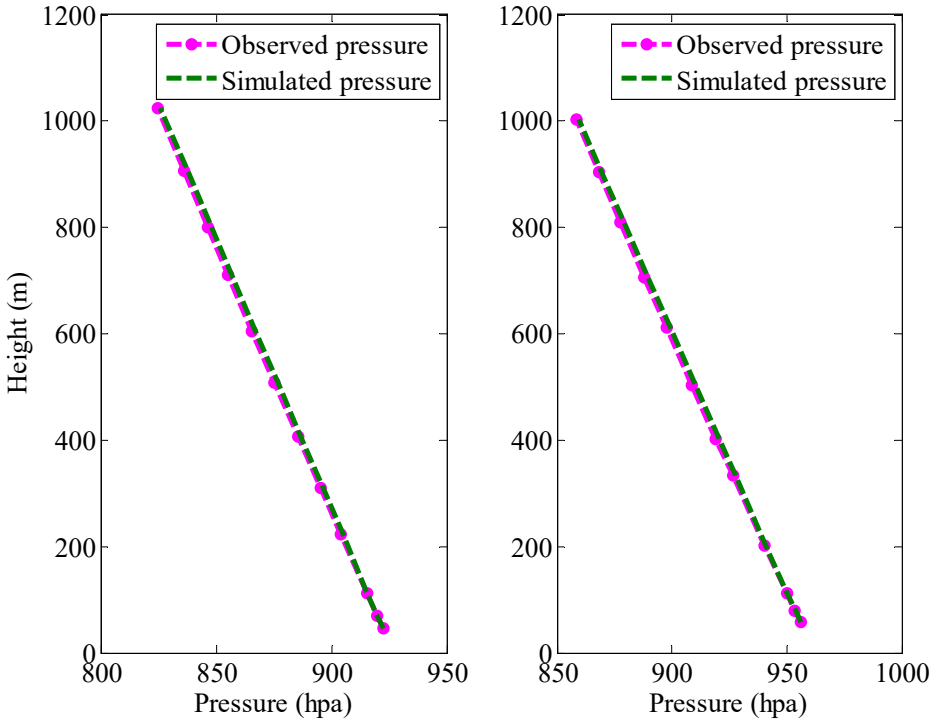

188

189 **Fig. 6.** Comparison between the simulated and observed pressures corresponding to two dropsondes during

190 hurricane Katrina (Left: 051926170 and Right: 051926111)

191 It is interesting to notice that the developed pressure formula of Eq. (9) may offer an

192 improved method to assess the climate change impacts on the wind field of tropical cyclones. More

193 specifically, the climate change assessment could be considered in terms of the surface central

194 pressure and the vertical pressure profile. Based on the surface central pressure, the future

195 projections of the sea surface temperatures (SST) can be incorporated into the wind field

196 simulations using the relative intensity developed by Darling (1991). Recently, Mudd et al. (2014)

197 carried out simulations to quantify the climate change impact on the northeast US coastal region

198 with this methodology. As pointed out by Mudd et al. (2015), however, considering only the SST

199 will not give accurate results for climate change estimation. Several other environmental

200 parameters that can contribute significantly to the tropical cyclone intensity and are expected to

201 change with global warming, should be accounted for (e.g., air moisture content, temperature at

202 higher altitudes). For example, the moisture content is believed to increase significantly with
203 global warming (IPCC 2000; 2007; 2012). This indicates reduced lapse rates (Frierson 2005),
204 which could be conveniently integrated into the wind field simulations with the proposed 2-D
205 pressure model.

206 **3. Height-resolving wind field**

207 A linear height-resolving wind field model recently developed by Snaiki and Wu (2016) will be
208 used in this study for wind field simulation. The model not only considers the radial variation of
209 the depth scale of the boundary layer but also accounts for the azimuthal dependence of wind field,
210 resulting an enhanced simulation of the real behavior of a moving tropical cyclone (Snaiki and Wu
211 2016). In this section, a brief discussion of the employed wind field model will first be presented
212 for completeness, followed with the improved wind field simulation by integrating the 2-D
213 pressure field.

214 The governing equation of the wind field could be described as follows:

215 $$\frac{\partial \boldsymbol{v}}{\partial t} + \boldsymbol{v}.\nabla \boldsymbol{v} = -\frac{1}{\rho}\nabla p - f\boldsymbol{k} \times \boldsymbol{v} + \boldsymbol{F} \tag{13}$$

216 where $\boldsymbol{v}$ = wind velocity; f = Coriolis parameter; $\boldsymbol{k}$ = unit vector in the vertical direction; and $\boldsymbol{F}$ =
217 frictional force. In order to solve Eq. (13), the decomposition method is used in which the wind
218 velocity ($\boldsymbol{v}$) is expressed as:

219 $$\boldsymbol{v} = \boldsymbol{v}_g + \boldsymbol{v}' \tag{14}$$

220 where $\boldsymbol{v}_g$ = gradient wind in the free atmosphere; and $\boldsymbol{v}'$ = frictional component near the ground
221 surface. Therefore two equations can be derived from Eq. (13):

$$\frac{\partial \boldsymbol{v}_g}{\partial t} + \boldsymbol{v}_g.\nabla \boldsymbol{v}_g = -\frac{1}{\rho}\nabla p - f\boldsymbol{k} \times \boldsymbol{v}_g \tag{15a}$$

$$\frac{\partial \boldsymbol{v}'}{\partial t} + \boldsymbol{v}'.\nabla \boldsymbol{v}' + \boldsymbol{v}'.\nabla \boldsymbol{v}_g + \boldsymbol{v}_g.\nabla \boldsymbol{v}' = -f\boldsymbol{k} \times \boldsymbol{v}' + \boldsymbol{F} \tag{15b}$$

Similar to Meng et al. (1995), the gradient wind pattern $\boldsymbol{v}_g$ is assumed to move at the translation velocity of the tropical cyclone c in the free atmosphere, thus the unsteady term can be expressed as: $\frac{\partial \boldsymbol{v}_g}{\partial t} = -\boldsymbol{c}.\nabla \boldsymbol{v}_g$. On the other hand, the unsteady term $\frac{\partial \boldsymbol{v}'}{\partial t}$ in the tropical cyclone boundary layer is usually considered significantly smaller than the turbulent viscosity and inertia terms, and hence neglected.

3.1 Gradient wind speed

Equation (15a) could be solved straightforwardly in the cylindrical coordinate system (Georgiou 1985; Meng et al. 1995). Hence:

$$v_{\theta g} = \frac{\left(-csin\left(\theta - \upsilon\right) - fr\right)}{2} + \left[\frac{\left(-csin\left(\theta - \upsilon\right) - fr\right)^2}{4} + \frac{r}{\rho}\frac{\partial p}{\partial r}\right]^{1/2} \tag{16}$$

where υ = approach angle (counter clockwise positive from the East). The radial velocity is then obtained from the continuity equation: $v_{rg} = -\frac{1}{r}\int_0^r \frac{\partial v_{\theta g}}{\partial \theta} dr$ which is usually disregarded as suggested by Meng et al. (1995) due to its insignificant effects.

3.2 Frictional wind speed

In the cylindrical coordinate, Eq. (15b) becomes:

$$u'\frac{\partial u'}{\partial r} + \frac{v_{\theta g} + v'}{r}\frac{\partial u'}{\partial \theta} + w\frac{\partial u'}{\partial z} - \frac{v'^2}{r} - \xi_g v' = K\left[\nabla^2 u - \frac{1}{r^2}\left(u + 2\frac{\partial v}{\partial \theta}\right)\right] \tag{17a}$$

$$u'\frac{\partial v'}{\partial r}+\frac{v_{\theta g}+v'}{r}\frac{\partial v'}{\partial \theta}+w\frac{\partial v'}{\partial z}+\frac{u'v'}{r}+\xi_{ag}u'+\frac{v'}{r}\frac{\partial v_{\theta g}}{\partial \theta}=K\left[\nabla^2 v-\frac{1}{r^2}\left(v-2\frac{\partial u}{\partial \theta}\right)\right] \quad (17b)$$

where (u,v,w) = velocity vector; u',v' = frictional components of the wind velocity; $\xi_g=\frac{2v_{\theta g}}{r}+f$ is the absolute angular velocity; $\xi_{ag}=\frac{\partial v_{\theta g}}{\partial r}+\frac{v_{\theta g}}{r}+f$ is the vertical component of absolute vorticity of the gradient wind; and K = the turbulent diffusivity that is assumed to be a constant in this study.

The nonlinear Eqs. (17a) and (17b) could first be simplified using the scale analysis, and then linearized as:

$$\frac{v_{\theta g}}{r}\frac{\partial u'}{\partial \theta}-\xi_g v'=K\frac{\partial^2 u'}{\partial z^2} \quad (18a)$$

$$\frac{v_{\theta g}}{r}\frac{\partial v'}{\partial \theta}+\xi_{ag}u'+\frac{v'}{r}\frac{\partial v_{\theta g}}{\partial \theta}=K\frac{\partial^2 v'}{\partial z^2} \quad (18b)$$

The analytical solution for this linear system is presented as follows (Snaiki and Wu 2016):

$$u'(\theta,z')=(\alpha/\beta)^{1/2}\times Real\left\{A_0\times e^{(q_0 z')}+A_1\times e^{(q_1 z'+i\theta)}+A_{-1}\times e^{(q_{-1}z'-i\theta)}\right\}=u_0+u_1+u_{-1} \quad (19a)$$

$$v'(\theta,z')=Imag\left\{A_0\times e^{(q_0 z')}+A_1\times e^{(q_1 z'+i\theta)}+A_{-1}\times e^{(q_{-1}z'-i\theta)}\right\}=v_0+v_1+v_{-1} \quad (19b)$$

where $\alpha=\frac{1}{2K}\xi_g$; $\beta=\frac{1}{2K}\xi_{ag}$; $q_1=-(1+i)\left[\gamma+\sqrt{\alpha\beta}-\phi\right]^{1/2}$; $q_{-1}=-(1+i)\left[-\gamma+\sqrt{\alpha\beta}-\phi\right]^{1/2}$; $q_0=-(\alpha\beta)^{1/4}$; $\gamma=\frac{1}{2K}\frac{v_{\theta g}}{r}$; $\phi=\frac{1}{2Kr}\frac{\partial v_{\theta g}}{\partial \theta}$; and z' = new vertical coordinate used as the base of the computation scheme where $z'=0$ is located above z_{10} (the 10 m height above the mean height of roughness elements) (Meng et al. 1995). The other parameters are presented as follows:

$$A_0=\frac{-X_3}{X_1+X_2X_4} \quad (20a)$$

$$A_1 = \frac{icC_d e^{-i\upsilon}}{4K\left(q_1 - q_{-1}^{*}\right)}\left(A_0 + A_0^{*}\right) \tag{20b}$$

$$A_{-1} = \frac{icC_d e^{i\upsilon}}{4K\left(q_1^{*} - q_{-1}\right)}\left(A_0 + A_0^{*}\right) \tag{20c}$$

$$X_1 = \left[q_0 + \frac{fr}{K}C_d - \frac{2\eta C_d}{K} - \frac{c^2 {C_d}^2}{4K^2\left(q_1 - q_{-1}^{*}\right)} + \frac{c^2 {C_d}^2}{4K^2\left(q_1^{*} - q_{-1}\right)}\right] \tag{20d}$$

$$X_2 = \left[-q_0^{*} - \frac{fr}{K}C_d + \frac{2\eta C_d}{K} - \frac{c^2 {C_d}^2}{4K^2\left(q_1 - q_{-1}^{*}\right)} + \frac{c^2 {C_d}^2}{4K^2\left(q_1^{*} - q_{-1}\right)}\right] \tag{20e}$$

$$X_3 = -2\frac{iC_d}{K}\left(\eta - \frac{fr}{2}\right)^2 \tag{20f}$$

$$X_4 = -\left[-q_0 - \frac{fr}{2K}C_d + \frac{\eta C_d}{K}\right] \Big/ \left[-q_0^{*} - \frac{fr}{2K}C_d + \frac{\eta C_d}{K}\right] \tag{20g}$$

$$\eta = \left[\frac{\left(-csin\left(\theta - \upsilon\right) - fr\right)^2}{4} + \frac{r}{\rho}\frac{\partial p}{\partial r}\right]^{1/2} \tag{20h}$$

where C_d = drag coefficient; and (*) indicates a complex conjugate.

3.3 An improved wind field simulation for tropical cyclone

As mentioned in the preceding sections, the solution of the wind field could be conveniently obtained by prescribing a pressure field that is unchanged with height (e.g., Meng et al. 1996; Kepert 2001; Snaiki and Wu 2016). If the pressure variation with respect to the height is considered, various gradient wind values corresponding to different heights need to be calculated. This also leads to the mutual dependence of the gradient wind speed and the boundary layer depth. To obtain the accurate value of the gradient wind in the wind field simulation of the tropical cyclone, the iteration approach is utilized herein. In Snaiki and Wu (2016), the depth scale of the tropical cyclone was highlighted to give good estimate of the height where turbulent fluxes tend

to become negligible. Specifically, three depth scales of the tropical cyclone, namely $\delta_0 = 1\Big/(\alpha\beta)^{\frac{1}{4}}$, $\delta_1 = 1\Big/\left[\gamma+\sqrt{\alpha\beta}-\phi\right]^{\frac{1}{2}}$ and $\delta_{-1} = 1\Big/\left[-\gamma+\sqrt{\alpha\beta}-\phi\right]^{\frac{1}{2}}$ corresponding to the frictional components (u_0, v_0), (u_1, v_1) and (u_{-1}, v_{-1}) [Eq. (19)], respectively, have been defined. Since, (u_0, v_0) are the dominant frictional component, it is reasonable to select δ_0 as the initial value of the height of the boundary layer. A systematic way to calculate the height-resolving wind field in this study is illustrated in Fig. 7.

The first part of the flow chart of Fig. 7 is to determine the initial estimate of the boundary layer height δ_0. Since δ_0 and the gradient wind speed depend on each other, the iteration process is necessary. Once the initial guess for the boundary layer height δ_0 is determined, the corresponding frictional wind speed components could be evaluated. The boundary layer height will be updated until the contribution from the friction become negligible. Based on the obtained boundary layer height δ_i, the wind field at certain height will be calculated using two different formulas. A constant value of the gradient wind speed evaluated at δ_i is utilized for the locations below the boundary layer height (i.e., $z < \delta_i$). Otherwise (i.e., $z > \delta_i$), the gradient wind speed is a function of height z, and the frictional components are equal to zero.

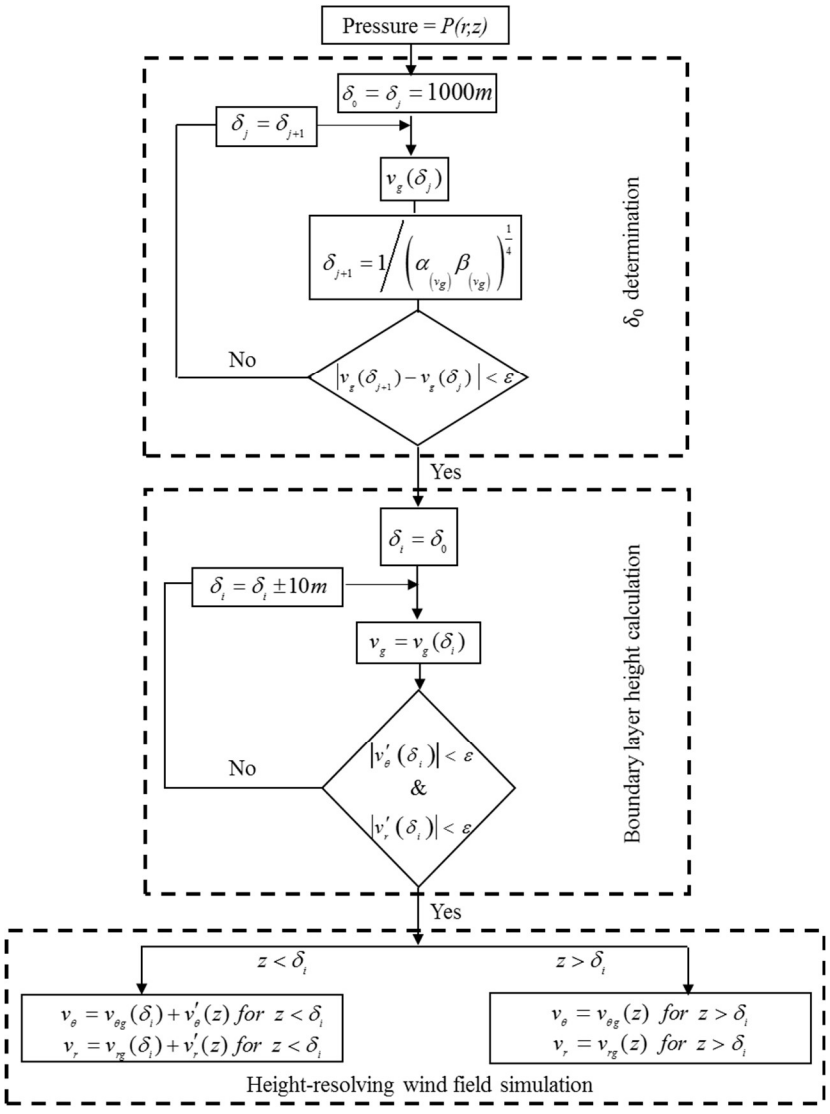

Fig. 7. Flow chart of wind field simulation methodology

A simple wind field simulation example is presented in Fig. 8, where $p_{c0} = 940\,hpa$; $r_m = 40\,km$; $B = 1.2$; $c = 10\,m/s$; $z_0 = 0.0001$; $k_m = 50m^2/s$; and $\upsilon = 90°$, to highlight the importance of considering the accurate gradient wind speed and boundary layer depth by iteration method. The standard method indicates a constant value of the gradient wind speed is employed in the wind field simulation.

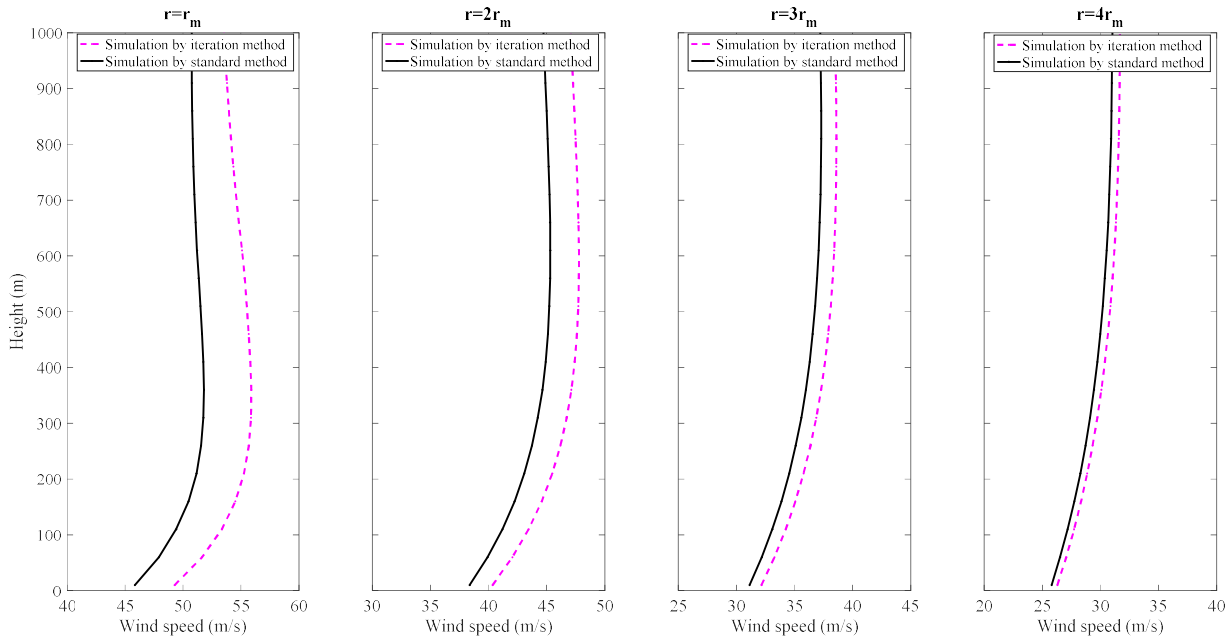

Fig. 8. Simulation of the vertical wind profiles at different locations

As shown in Fig. 8, the vertical wind profiles simulated using the iteration and standard schemes present large difference. The difference becomes more significant as the location is close to the radius of maximum wind and tends to decrease far away from the center of the tropical cyclone. It should be mentioned that the tangential wind speed $v_{\theta g}$ in Huang et al. (2012) was considered to vary with height from the ground surface rather than evaluated at the boundary layer depth, which may need further improvement.

4. Model Validation

Wind records were obtained from the National Hurricane Center's North Atlantic Hurricane Database (HURDAT). Typically, the parameters needed for the simulation are: υ approach angle; c translation velocity of the hurricane; p_c central pressure; Δp central pressure difference; $R_{\max}$ radius of maximum winds; B Holland's parameter; ψ latitude; and λ longitude. The parameter $R_{\max}$ and B can be estimated using the methods available in the literature (e.g., Powell et al., 1991;

1998; Anthes 1982; Vickery et al., 2000b; Holland, 2008). In this study, the necessary information is supplemented by the H*Wind snapshots. For the lapse rate parameters, the coefficients Γ_{r_m}, Γ_{eye} and Γ_0 can be approximated using the dropsonde data.

4.1 Surface wind simulation and validation

Two hurricanes, namely hurricane Bertha (1996) and Fran (1996) were selected for the surface wind validation purpose. The 10 min averaged time was used for the observed wind data at 10 m height for both hurricanes.

4.1.1 Hurricane Bertha

The anemometer is located on the FPSN7 station at (N33.44° , W77.74°). The parameters B and R_{max} were found to be: $B = 1.2$ and $R_{max} = 70\,km$. The observed wind speeds and directions were compared with those obtained using the improved wind field model, and good agreement is presented as in Fig. 9.

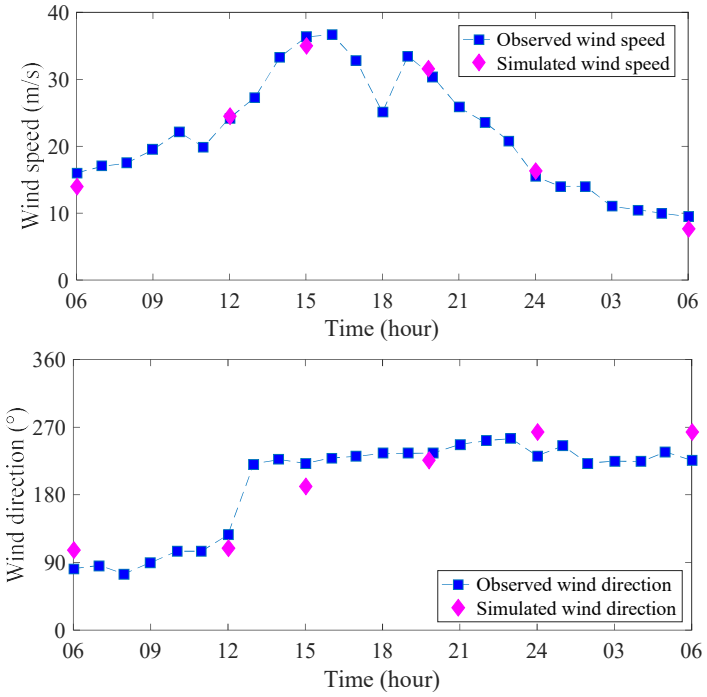

Fig. 9. Observed and simulated wind speeds (top) and directions (bottom) at FPSN 7, Hurricane Bertha

4.1.2 Hurricane Fran

The necessary parameters for the simulation were recorded by the marine station FPSN7 from September 5th to September 6th. The station ID is 41013, located at (N33.44°, W77.74°). For hurricane Fran B=0.95 and $R_{max} = 85\,km$. As shown in Fig. 10, the results generated by the present wind field model are consistent with hurricane Fran observations.

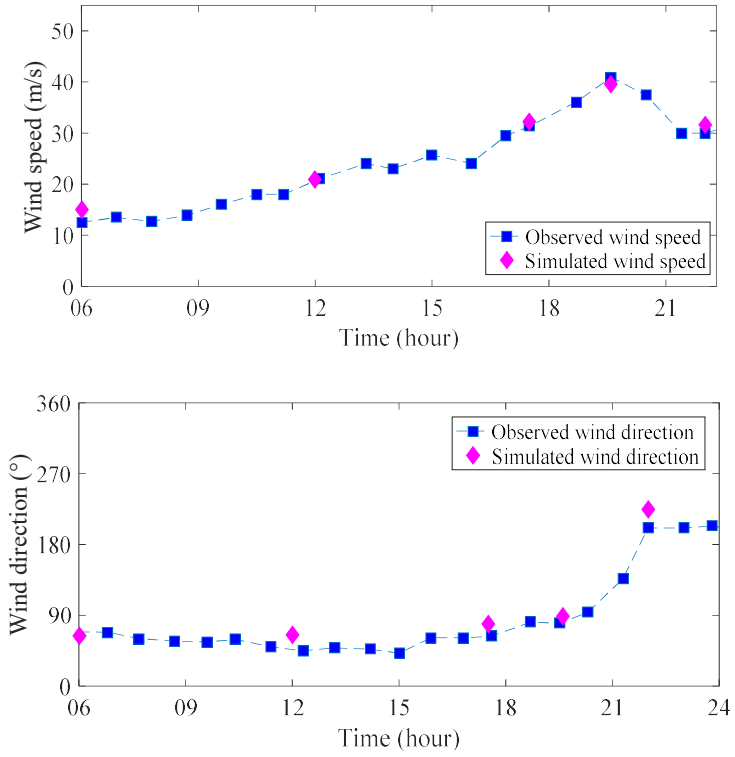

Fig. 10. Observed and simulated wind speeds (top) and directions (bottom) of Hurricane Fran

4.2 Vertical wind profile simulation and validation

Wind records from hurricane Bertha and Katrina were used to highlight the effects of the proposed 2-D pressure field on the tropical cyclone winds. Simulation vertical wind profiles of hurricane Bertha in the eye-wall and outer-vortex regions were compared with the averaged wind profiles obtained by Franklin et al. (2003). On the other hand, normalized wind profiles obtained by dropsondes data were used to validate simulation vertical wind profiles of hurricane Katrina.

4.2.1 Hurricane Bertha

Comparison between mean wind speed profiles in the eye-wall and outer-vortex regions for a specific hurricane is demonstrated to be very challenging. Franklin et al. (2003) constructed the averaged wind profile based on numerous observations involving several hurricanes. By averaging a large number of wind profiles from various hurricanes, good insight on the vertical profile of a typical tropical cyclone could be obtained.

Several vertical wind profiles for hurricane Bertha at various locations of the eye-wall and outer-vortex regions were constructed based on the improved wind field simulation. As shown in Fig. 11, the simulation profiles present good agreement with the averaged one obtained by Franklin et al. (2003) for both regions. Furthermore, it is noted that there is an obvious super-gradient region for the eye-wall wind profiles (e.g., Kepert 2000; Kepert and Wang 2001; Snaiki and Wu 2016).

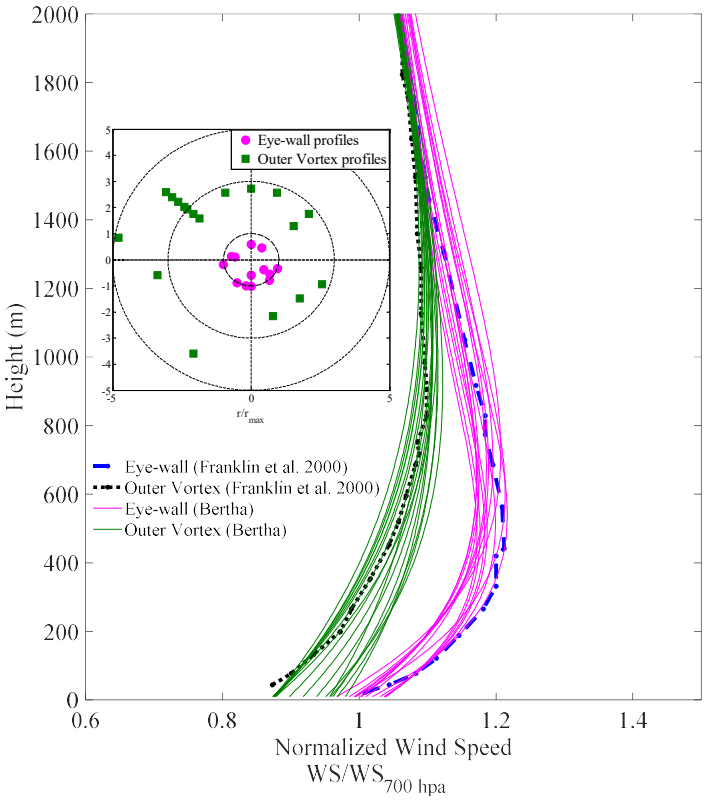

Fig. 11. Wind profiles in the eye-wall and outer vortex regions

4.2.2 Hurricane Katrina

Wind records form dropsondes (051926111) and (044535004) launched during hurricane Katrina (2005) were used to validate the simulated wind profiles. In the comparison the wind profiles were both normalized by a reference wind speed at 500 m. It should be noted that dropsondes only provide the instantaneous wind speed profiles. Hence, more emphasis will be given to the high-altitude comparison of observed and simulated results, where the mechanical turbulence is smaller. To assess the effects of the proposed 2D pressure field on the wind profiles, the simulation results based on the Holland's conventional pressure field are also presented. As indicated in Fig. 12, the consideration of the proposed 2D pressure profile results in more accurate simulation of the wind speeds.

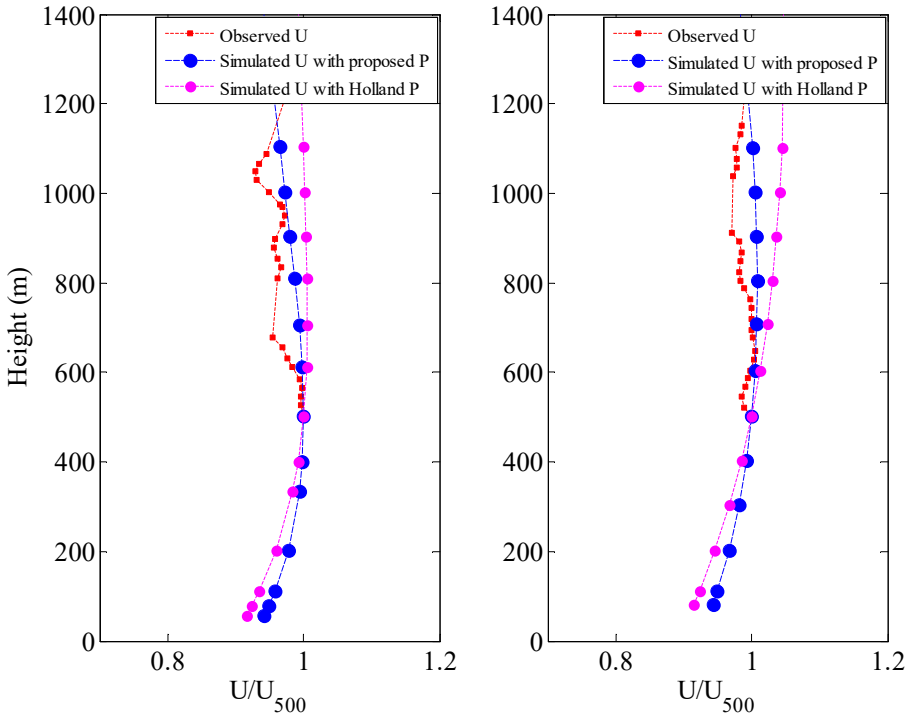

Fig. 12. Comparison of the normalized vertical wind profiles corresponding to two dropsondes during hurricane Katrina (Left: 051926111 and Right: 044535004)

363 Furthermore, the simulated wind profiles plotted in Fig. 13 clearly present the significant
364 importance of an accurate pressure field on the wind field simulations.

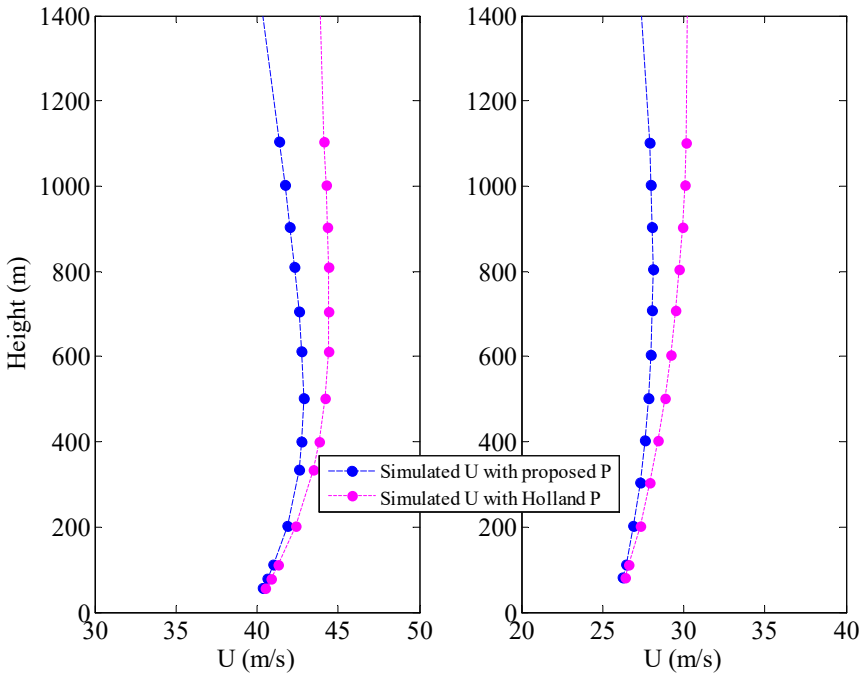

365

366 **Fig. 13.** Comparison of the vertical wind profiles corresponding to two dropsondes during hurricane Katrina (Left:
367 051926111 and Right: 044535004)

368 **5. Concluding remarks**

369 A 2-D pressure model was proposed in this study, where the effects of temperature and moisture
370 were simultaneously accounted for through the virtual temperature. Furthermore, the linearized
371 consideration of the virtual temperature with respect to the height was introduced in the pressure
372 formula through the temperature lapse rate parameter. The empirical formulas constructed for
373 considering the spatial variation of the temperature lapse rate in the tropical cyclones greatly
374 simplified the simulations of pressure field. Then a framework based on the height-resolving
375 methodology was established to integrate the proposed 2-D pressure field into the boundary layer
376 wind field simulations of translating tropical cyclones. The improved wind field model involves

the iteration approach to systematically select an appropriate height for the calculation of gradient wind speed, hence, it offers better simulation results that are more consistent with the tropical cyclone observations. The improved height-resolving wind field simulations can be used in conjunction with the Monte Carlo techniques to perform risk analysis of tropical cyclone hazards. In addition, the present model also shows great promise in offering an improved method (based on the proposed 2-D pressure field) to assess the climate change impacts on the wind field by including some essential environmental parameters (e.g., temperature profile, moisture content).

Acknowledgements

The support for this project provided by the NSF Grant # CMMI 15-37431 is gratefully acknowledged.

References

Anthes, R.A., (1982). "Tropical Cyclones: Their Evolution, Structure, and Effects", American Meteorological Society, Boston, USA.

(CCSP) US Climate Change Science Program, (2006). "Temperature Trends in the Lower Atmosphere: Steps for Understanding and Reconciling Differences (ed: T R Karl, S J Hassol, C D Miller and W L Murray), A Report by the Climate Change Science Program and the Subcommittee on Global Change Research, Washington, DC.

Darling, R.W. R., (1991). "Estimating probabilities of hurricane wind speeds using a large scale empirical model.", J. Clim., 4(10), 1035–1046.

Franklin, J. L., M. L. Black, and K. Valde, (2003). "GPS dropwindsonde wind profiles in hurricanes and their operational implications", Wea. Forecasting, 18, 32–44.

Frierson, D. M. W., (2005). "Studies of the General Circulation of the Atmosphere with a Simplified Moist General Circulation Model", Ph.D. thesis, Princeton University, pp. 218.

401 Galchen, T. and Somerville, R.C.J., (1975). “On the use of a coordinate transformation for the solution of Navier-
402 Stokes equations”, Journal of Computational Physics, Vol. 17, pp. 209–228.
403 Georgiou, P.N., (1985). “Design Wind Speeds in Tropical Cyclone-Prone Regions”, PhD Thesis, University of
404 Western Ontario, London, Ontario, Canada.
405 HURDAT, (2013). Atlantic basin hurricane database. Atlantic Oceanographic and Meteorological Laboratory
406 (AOML). National Oceanic and Atmospheric Administration (NOAA).
407 Hock, T. F., and J. L. Franklin, (1999). “The NCAR GPS dropwindsonde”, Bull. Amer. Meteor. Soc., 80, 407–420.
408 Holland, G.J., (1980). “An analytical model of the wind and pressure profile in hurricanes”, Monthly Weather Review,
409 Vol. 108, No. 8, pp. 1212–1218.
410 Holland, G.J., (2008). “A revised hurricane pressure–wind model”, Monthly Weather Review, Vol. 136, pp. 3432–
411 3445.
412 Huang, W.F. and Xu, Y.L., (2012). “A refined model for typhoon wind field simulation in boundary layer”, Advances
413 in Structural Engineering, 15(1), 77-89.
414 (IPCC) Intergovernmental Panel on Climate Change, (2000). “Emissions scenarios.”, A Special Rep. of Working
415 Group III, Geneva, Switzerland.
416 (IPCC) Intergovernmental Panel on Climate Change, (2007). “Climate change 2007: Synthesis report.”, Contribution
417 of Working Groups I, II and III to the Fourth Assessment Rep. of the Intergovernmental Panel on Climate Change,
418 R. K. Pachauri and A. Reisinger, eds., Geneva, Switzerland, 104.
419 (IPCC) Intergovernmental Panel on Climate Change, (2012). “Changes in climate extremes and their impacts on the
420 natural physical environment.”, Managing the risks of extreme events and disasters to advance climate change
421 adaptation.
422 Kepert, J. D., (2001). “The dynamics of boundary layer jets within the tropical cyclone core. Part I: Linear theory.”,
423 J. Atmos. Sci., 58(17), 2469–2484.
424 Kowalski A. S. & Sanchez-Cañete E. P., (2010). “A New Definition of the Virtual Temperature, Valid for the
425 Atmosphere and the CO2 -Rich Air of the Vadose Zone”, Journal of Applied Meteorology and Climatology, 49:
426 1692-1695.
427 Lee, K. H., and Rosowsky, D. V., (2007). “Synthetic hurricane wind speed records: Development of a database for
428 hazard analysis and risk studies.”, Nat. Hazard. Rev., 10.1061.

Meng, Y., Matsui, M. and Hibi, K., (1995). “An analytical model for simulation of the wind field in a typhoon boundary layer”, Journal of Wind Engineering and Industrial Aerodynamics, Vol. 56, No. 2–3, pp. 291–310.

Meng, Y., Matsui, M. and Hibi, K., (1997). “A numerical study of thewind field in a typhoon boundary layer”, Journal of Wind Engineering and Industrial Aerodynamics, Vol. 67–68, pp. 437–448.

Mudd, L., Wang, Y., Letchford, C., and Rosowsky, D., (2014). “Assessing climate change impact on the U.S. east coast hurricane hazard: Temperature, frequency, and track.”, Nat. Hazards Rev., 10.1061.

Mudd, L., Letchford, C., Rosowsky, D. and Lombardo, F., (2015). “A Probabilistic Hurricane Rainfall Model and Possible Climate Change Implications. ”, Proceedings of the 14th International Conference on Wind Engineering (ICWE14), June 2015, Porto Alegre, Brazil.

Nishijima, K., Maruyama, T., and Graf, M., (2012). “A preliminary impact assessment of typhoon wind risk of residential buildings in Japan under future climate change.”, Hydrol. Res. Lett., 6(1), 23–28.

Powell, M. D., Dodge, P. P., and Black, L. B., (1991). ‘‘The landfall of Hurricane Hugo in the Carolinas: Surface wind distribution.’’, Weather and Forecasting, 6, 379–399.

Powell, M. D., Houston, S. H., Amat, L. R., and Morisseau-Leroy, N., (1998). “The HRD real-time hurricane wind analysis system.”, J. Wind Eng. Ind. Aerodyn., 77–78, 53–64

Powell, M. D., Vickery, P. J., and Reinhold, T. A., (2003). “Reduced drag coefficient for high wind speeds in tropical cyclones”, Nature, 422, 279–283, doi: 10.1038/nature 01481

Rosenthal, S.L., (1962). “A Theoretical Analysis of the Field of Motion in the Hurricane Boundary Layer”, NHRP Report No. 56, Department of Commerce, USA.

Russell, L.R., (1968) “Probability distribution for Texas gulf coast hurricane effects of engineering interest”, Ph.D. Thesis, Stanford University.

Russell, L.R., (1971). “Probability distributions for hurricane effects”, J. Waterw., Harbors, Coastal Eng. Div. 97, 139–154.

Schär, C., D. Leuenberger, O. Fuhrer, D. Lu¨thi, and C. Girard, (2002). “A new terrain-following vertical coordinate formulation for atmospheric prediction models”, Mon. Wea. Rev., 130, 2459–2480

Shapiro, L.J., (1983). “The asymmetric boundary layer flow under a translating hurricane”, Journal of the Atmospheric Sciences, Vol. 40, No. 8, pp. 1984–1998.

Smith, R. K., (1968). “The surface boundary layer of a hurricane”. Tellus, 20, 473-483

457 Smith, R. K., (2003). “A simple model of the hurricane boundary layer”, Quart. J. Roy. Meteor. Soc., 129, 1007-1027
458 Snaiki, R., Wu, T., (2016). “Temperature and Moisture Effects on the Tropical Cyclone Boundary Layer: Pressure
459 and Wind”, Proceedings of 8th International Colloquium on Bluff-Body Aerodynamics and its Application
460 (BBAAVIII), June, 2016, Boston, USA.
461 Tryggvason, V.J., Davenport, A.G., Surry, D., (1976). “Predicting Wind-Induced Response in Hurricane Zones”,
462 Journal of the Structural Division, 102, p.2333-2350.
463 Vickery, P. J., Skerlj, P. F., and Twisdale, L. A., (2000b). “Simulation of hurricane risk in the U.S. using empirical
464 track model.”, J. Struct. Eng., 10.1061.
465 Vickery, P. J., Masters, F. J., Powell, M. D., and Wadhera, D., (2009a). “Hurricane hazard modeling: The past, present
466 and future.”, J. Wind Eng. Ind. Aerodyn., 97(7–8), 392–405.
467 Vogl S. and R. K. Smith, (2009). “Tropical Cyclone Boundary-Layer Models”, PhD Thesis, LMU Munich, Munich
468 Germany.
469 Willoughby, H. E., Darling, R. W. R., and Rahn, M. E., (2006): “Parametric representation of the primary hurricane
470 vortex. Part II: A new family of sectionally continuous profiles”, Monthly Weather Review, 134, pp. 1102–1120.
471 Yoshizumi, S., (1968). “On the asymmetry of wind distribution in the lower layer of a typhoon”, Journal of the
472 Meteorological Society of Japan, Vol. 46, No. 3, pp. 153–159.
473 Zhao, L., Lu, A., Zhu, L., Cao, S. and Ge, Y., (2013): “Radial pressure profile of typhoon field near ground surface
474 observed by distributed meteorologic stations”, Journal of Wind Engineering and Industrial Aerodynamics, 122,
475 pp.105-112.